

# Analytical test statistic distributions of the MMME eigenvalue-based detector for spectrum sensing

Martijn Arts, Andreas Bollig and Rudolf Mathar  
Institute for Theoretical Information Technology  
RWTH Aachen University  
D-52074 Aachen, Germany  
Email: {arts, bollig, mathar}@ti.rwth-aachen.de

**Abstract**—We present an analytical derivation of the probability density functions (PDFs) of the maximum-minus-minimum eigenvalue (MMME) detector for the special case of two cooperating secondary users (SUs) in a spectrum sensing scenario. For this we employ a simple additive white Gaussian noise (AWGN) model, where in general  $K$  cooperating SUs are monitoring the wireless spectrum to determine the presence of a single primary user, which transmits phase shift keying (PSK) modulated signals. The sample covariance matrix is a Wishart matrix under both the noise only and the signal plus noise hypothesis under this model. For  $K = 2$ , we derive the exact PDFs for the MMME detector under both hypotheses for a finite number of samples  $N$  taken. Then, we compare the performance of the MMME detector and the maximum-minimum eigenvalue (MME) detector aided by exact PDFs available in the literature for this model. Finally, we analyze the noise power uncertainty tolerance margin of the MMME detector under which it shows superior performance to the MME detector.

## I. INTRODUCTION

Modern mobile multimedia streaming services put a huge demand for high data rates on wireless telecommunication systems. This demand is expected to continually increase in the coming years, as the number of mobile Internet users is steadily growing. However, de facto all interesting frequency bands are already licensed at the moment and adoption of such spectral bands is only possible by termination of existing licenses, which is an accountability of governmental agencies. Since in practice large parts of the spectrum are not continually in use at specific locations and at certain points in time, it was proposed to reuse these currently unoccupied spectral bands for unlicensed users. In the literature such techniques can be subsumed under the term dynamic spectrum access, see e.g. [1]. If the unlicensed users, called secondary users (SUs), autonomously decide about communicating on licensed spectral bands, they perform opportunistic spectrum access. It is directly clear, that it is of utmost importance to prevent SUs from creating significant interference for licensed primary users (PUs).

The process of detecting transmission opportunities for SUs is called *spectrum sensing*. Various detection strategies

This work was partly supported by the Deutsche Forschungsgemeinschaft (DFG) project CoCoSa (grant MA 1184/26-1).

978-1-4673-6540-6/15/\$31.00 ©2015 IEEE

have been proposed in the literature, which assume different amounts of knowledge about the PU signal and therefore differ in the signal features used for detection, see [2] for a review. Typically, the noise present in communication systems is assumed to be uncorrelated. In contrast to this, a signal transmitted by a PU which is observed by multiple cooperating SUs shows correlation. This motivates the application of detectors based on the sample covariance matrix, see for instance [3]–[7]. Of special interest in this work are two simple detectors, which rely on the two extreme eigenvalues of the sample covariance matrix. The test statistic of the maximum-minimum eigenvalue (MME) detector is defined as [3], [4]:

$$T = \frac{\lambda_1}{\lambda_K}, \quad (1)$$

where  $\lambda_1$  and  $\lambda_K$  are the biggest and the smallest eigenvalue of a sample covariance matrix which was generated from the observations of  $K$  cooperating SUs with  $N$  number of samples. A very similar test statistic was introduced in [7], the maximum-minus-minimum eigenvalue (MMME) detector:

$$D = \lambda_1 - \lambda_K. \quad (2)$$

Recent advances in *Random Matrix Theory* (RMT) enable the investigation of exact distributions of the eigenvalues of so called Wishart matrices, see e.g. [8]. Such Wishart matrices occur for instance when a Gaussian random matrix  $\mathbf{A}$  is multiplied with its hermitian, i.e.,  $\mathbf{A}\mathbf{A}^H$ . In a communication context this is relevant in the analysis of the multiple-input multiple-output (MIMO) correlation matrix [9] and also for the analysis of detectors based on the eigenvalues of sample covariance matrices in spectrum sensing applications [10].

In this work, we derive the probability density functions (PDFs) of the MMME test statistic under both the noise only as well as the signal plus noise hypothesis. This is done for the special case of two cooperating SUs under a simple additive white Gaussian noise (AWGN) model featuring a single phase shift keying (PSK) modulated PU signal. Since the PDFs of the MME detector are available under the same model from literature [11], a direct analytical performance comparison is possible.

In Section II we specify our system model and define notation. Section III focuses on the PDFs of the two detectors

MME and MMME. After summarizing existing results for the MME detector in Section III-A, we derive the PDFs of the MMME detector in Section III-B under both Hypotheses. Based on these analytical results, a performance comparison is conducted in Section IV. Since the MMME detector has a dependency on the noise power we evaluate how much noise power uncertainty can be tolerated such that the MMME detector performs favorably when compared to the MME detector in Section V.

## II. SYSTEM MODEL

In spectrum sensing, deciding whether a PU is present can be cast as a binary hypothesis testing problem. Assuming additive noise, we can formalize this problem as:

$$\begin{aligned}\mathcal{H}_0 : \mathbf{y}(t) &= \mathbf{w}(t) \\ \mathcal{H}_1 : \mathbf{y}(t) &= \mathbf{x}(t) + \mathbf{w}(t).\end{aligned}$$

Here,  $\mathbf{y}(t)$  is a vector of complex baseband samples collected by the SUs at time index  $t \in \mathbb{N} = \{1, 2, \dots\}$  of dimension  $K \times 1$ . The vectors  $\mathbf{x}(t)$  and  $\mathbf{w}(t)$ , describe the received PU signal (if present) and the noise, respectively. Thus, under  $\mathcal{H}_0$  no received signal is present, which means the PU is not present or not transmitting.

We assume that the PU is using a PSK signal and the SUs receive this signal subject to additive white Gaussian noise (AWGN). Furthermore, the SUs are assumed to have the same signal-to-noise ratio (SNR)  $\alpha$ , resulting in the same received signal power  $\sigma_x^2$ . Thus,  $\mathbf{x}(t) = \sigma_x s(t) \mathbf{1}_K$  describes the received PU signal at the SUs, where  $s(t) \in \mathbb{C}$  is a complex PSK symbol on the unit circle ( $|s(t)| = 1$ ) and  $\mathbf{1}_K$  is a column vector of dimension  $K$  containing only ones. The PSK symbols  $s(t)$  are assumed to be i.i.d. and to follow a uniform distribution with an arbitrary PSK alphabet as support. Each entry of the noise vector  $\mathbf{w}(t)$  is assumed to follow a complex circularly symmetric Gaussian distribution with variance  $\sigma_w^2$ , denoted as  $\mathcal{CN}(0, \sigma_w^2)$ . Signal and noise are assumed to be independent and likewise all entries of the noise vector are assumed to be independent from each other.

By combining  $N$  sample vectors into the sample matrix  $\mathbf{Y} = (\mathbf{y}(1), \mathbf{y}(2), \dots, \mathbf{y}(N))$ , we can grasp the model in a convenient matrix form. Defining the PU signal matrix  $\mathbf{X}$  and the noise matrix  $\mathbf{W}$  in the same way, we get  $\mathbf{Y} = \mathbf{X} + \mathbf{W}$  under  $\mathcal{H}_1$  and  $\mathbf{Y} = \mathbf{W}$  under  $\mathcal{H}_0$ . Thus, the sample covariance matrix follows as  $\mathbf{R}_y = \frac{1}{N} \mathbf{Y} \mathbf{Y}^H$ .

## III. TEST STATISTIC DISTRIBUTIONS

In this Section we summarize results on the test statistic distributions of the maximum-minimum eigenvalue detector and develop new results on the test statistic distribution of the maximum-minus-minimum eigenvalue detector. As a basis we will briefly summarize the distributions of the sample covariance matrix first. To simplify the results, we assume the noise power to be  $\sigma_w^2 = 1$ , so that the signal power equals the SNR directly ( $\sigma_x^2 = \alpha$ ) and furthermore consider an unnormalized version of the sample covariance matrix  $\mathbf{R} = \mathbf{Y} \mathbf{Y}^H$  in the following.

Under  $\mathcal{H}_0$ , it follows that  $\mathbf{R}_0 = \mathbf{W} \mathbf{W}^H$ , which is a complex uncorrelated central Wishart matrix of dimension  $K$  with  $N$  degrees of freedom [12]. We denote this as  $\mathbf{R}_0 \sim \mathcal{CW}_K(N)$ .

Under  $\mathcal{H}_1$ , we have  $\mathbf{R}_1 = (\mathbf{X} + \mathbf{W})(\mathbf{X} + \mathbf{W})^H$ . In [11], it was shown that  $\mathbf{R}_1$  is a complex uncorrelated non-central Wishart matrix of dimension  $K$  with  $N$  degrees of freedom. We will denote this as  $\mathbf{R}_1 \sim \mathcal{CW}_K(N, \mathbf{\Omega})$ . The so called non-centrality matrix  $\mathbf{\Omega}$  is a parameter depending on the SNR  $\alpha$  and the dimensions of the sample matrix  $\mathbf{Y}$ . It can be given as  $\mathbf{\Omega} = \mathbb{E}[\mathbf{R}_1] = \mathbb{E}[\mathbf{X} \mathbf{X}^H] = \alpha N \mathbf{1}_K \mathbf{1}_K^T$ .

Analytical results for both the MME test statistic PDFs as well as the MMME test statistic PDFs under both hypotheses can be developed by confining the model to  $K = 2$  SUs, which will be assumed to be the case for the remainder of this paper.

### A. MME test statistic distribution

Under hypothesis  $\mathcal{H}_0$ , the PDF of the test statistic  $T$ , see (1), for  $K = 2$  has been found in [13] as:

$$f_0(T) = \frac{\Gamma(2N)}{\Gamma(N)\Gamma(N-1)} \left(1 - \frac{1}{T}\right)^2 \left(\frac{1}{T}\right)^N \left(1 + \frac{1}{T}\right)^{-2N}, \quad (3)$$

for  $T \geq 1$  and  $f_0(T) = 0$  for  $T < 1$ .

Under hypothesis  $\mathcal{H}_1$ , the PDF of  $T$  for  $K = 2$  parameterized on the SNR  $\alpha$  has been reported in [11]:

$$f_1(T) = e^{-(2\alpha N)} (T-1) T^{(N-2)} \times \sum_{j=0}^{\infty} \frac{(T^j - 1) \Gamma(j + 2N - 1) (2\alpha N)^{(j-1)}}{j! \Gamma(j + N - 1) \Gamma(N - 1) (T + 1)^{(j+2N-1)}}, \quad (4)$$

for  $T \geq 1$  and  $f_1(T) = 0$  for  $T < 1$ .

Note, that the normalization factor of the sample covariance matrix  $\mathbf{R}_x$  is present in both eigenvalues and cancels out in the ratio. Also, for both PDFs (3) and (4) knowledge of the actual noise power is not necessary, as (3) depends on the number of samples  $N$  and (4) depends on  $N$  and the SNR  $\alpha$ .

### B. MMME test statistic distribution

In order to derive the PDFs of the test statistic  $D$ , see (2), we need the joint PDF of the ordered eigenvalues of the unnormalized sample covariance matrix  $\mathbf{R}$ , denoted as  $f_{\lambda}(\boldsymbol{\lambda})$ , under both hypotheses. Here,  $\boldsymbol{\lambda} = (\lambda_1, \lambda_2, \dots, \lambda_K)^T$  is the vector of the ordered eigenvalues of  $\mathbf{R}$ , so that  $\lambda_1 \geq \lambda_2 \geq \dots \geq \lambda_K$ . Then, since for  $K = 2$  it holds that  $\lambda_1 = \lambda_2 + D$ , the following transformation gives the desired PDF:

$$g(D) = \int_0^{\infty} f_{\lambda}(\lambda_2 + D, \lambda_2) d\lambda_2. \quad (5)$$

Under  $\mathcal{H}_0$ , a convenient representation of the joint PDF of the eigenvalues of the unnormalized sample covariance matrix  $\mathbf{R}_0$  can be found in [8]. Setting  $K = 2$ , we find that

$$f_{\lambda}(\boldsymbol{\lambda}) = \frac{(\lambda_1 - \lambda_2)^2 (\lambda_1 \lambda_2)^{(N-2)} e^{-(\lambda_1 + \lambda_2)}}{(N-1)! (N-2)!}. \quad (6)$$

Inserting (6) into the transformation (5) yields:

$$g_0(D) = \frac{D^2 e^{-D}}{(N-1)!(N-2)!} \int_0^\infty e^{-2\lambda_2} (\lambda_2 + D)^{(N-2)} \lambda_2^{(N-2)} d\lambda_2. \quad (7)$$

The definite integral can be found in [14] (3.383.8), so that after simplifying we arrive at:

$$g_0(D) = \frac{D^{(N+1/2)} \mathcal{K}_{(3/2-N)}(D)}{\sqrt{\pi} \Gamma(N) 2^{(N-3/2)}}, \quad (8)$$

for  $D \geq 0$  and  $g_0(D) = 0$  for  $D < 0$ . Here,  $\mathcal{K}_a(b)$  is the modified Bessel function of the second kind of order  $a$ .

As mentioned above, under  $\mathcal{H}_1$  the Wishart matrix  $\mathbf{R}_1$  depends on the non-centrality matrix  $\mathbf{\Omega} = \alpha N \mathbf{1}_K \mathbf{1}_K^T$ , which is a rank one matrix [11]. Thus, the vector of ordered eigenvalues  $\boldsymbol{\omega}$  of  $\mathbf{\Omega}$  can be given explicitly. For  $K = 2$ , it follows that  $\omega_1 = 2\alpha N$  and  $\omega_2 = 0$ . The joint PDF of the eigenvalues of the unnormalized sample covariance matrix  $\mathbf{R}_1$  has  $\boldsymbol{\omega}$  as a parameter, see [8]. Inserting the values for  $\boldsymbol{\omega}$  and  $K = 2$ , it follows:

$$f_{\boldsymbol{\lambda}}(\boldsymbol{\lambda}) = \frac{e^{-(2\alpha N)} e^{-(\lambda_1 + \lambda_2)} (\lambda_1 - \lambda_2) (\lambda_1 \lambda_2)^{(N-2)} |\mathbf{F}(\boldsymbol{\lambda}, \boldsymbol{\omega})|}{2\alpha N [(N-2)!]^2}. \quad (9)$$

There,  $|\mathbf{F}(\boldsymbol{\lambda}, \boldsymbol{\omega})|$  is the determinant of a matrix where the  $(i, j)$ -th entry is  ${}_0\mathcal{F}_1(N-1; \lambda_j \omega_i)$ , which is a standard generalized hypergeometric function, c.f. [14] (9.14.1). The determinant can be explicitly calculated to  $|\mathbf{F}(\boldsymbol{\lambda}, \boldsymbol{\omega})| = {}_0\mathcal{F}_1(N-1; 2\alpha N \lambda_1) - {}_0\mathcal{F}_1(N-1; 2\alpha N \lambda_2)$ . Inserting (9) into the transformation (5) yields:

$$g_1(D) = \frac{D e^{-D} e^{-(2\alpha N)}}{2\alpha N [(N-2)!]^2} \int_0^\infty e^{-(2\lambda_2)} \lambda_2^{(N-2)} (\lambda_2 + D)^{(N-2)} \times [{}_0\mathcal{F}_1(N-1; 2\alpha N (\lambda_2 + D)) - {}_0\mathcal{F}_1(N-1; 2\alpha N \lambda_2)] d\lambda_2. \quad (10)$$

To the best of our knowledge, the definite integral in (10) does not have a closed-form solution. Hence, we take a similar path to [11], [15] and rewrite the hypergeometric function in terms of the modified Bessel function of the first kind of order  $a$ , denoted as  $\mathcal{I}_a(b)$ , by using the identity  ${}_0\mathcal{F}_1(a+1; b) = a! b^{-(a/2)} \mathcal{I}_a(2\sqrt{b})$ . Furthermore, we proceed to replace the Bessel function by its series expansion  $\mathcal{I}_a(b) = \sum_{j=0}^\infty \frac{1}{j! \Gamma(j+a+1)} \left(\frac{b}{2}\right)^{(2j+a)}$ . After substituting  $\Lambda = \lambda_2/D$  and simplifying we obtain (11). There, we have also used that for  $a \in \mathbb{N}$  it holds that  $\Gamma(a) = (a-1)!$ . Both definite integrals in (11) can be found in terms of Tricomi's confluent hypergeometric function, which is a solution to Kummer's differential equation, denoted as  $\mathcal{U}(a, b, c)$ , see also [16] (13.2.5). Using this result, we finally arrive at (12) for  $D \geq 0$  and  $g_1(D) = 0$  for  $D < 0$ .

In contrast to the MME detector the MMME detector is dependent on the noise power  $\sigma_w^2$  as well as the typically present normalization factor of the sample covariance matrix  $\mathbf{R}_y$ . When considering the normalized sample covariance matrix  $\mathbf{R}_y$ , the eigenvalues  $\boldsymbol{\lambda}$  must be scaled by  $1/N$  compared to the unnormalized case discussed above. Similarly, a noise power  $\sigma_w^2 \neq 1$ , results in a scaling factor  $\sigma_w^2$  for the eigenvalues.

Hence, using the simple transformation  $\hat{D} = \frac{\sigma_w^2}{N} D$  on the PDFs (8) and (12), i.e.,  $\hat{g}(\hat{D}) = \frac{N}{\sigma_w^2} g\left(\frac{\hat{D}N}{\sigma_w^2}\right)$ , yields the desired PDFs (13) and (14) for  $D \geq 0$ . Note, that  $\hat{g}_0(\hat{D}) = 0$  and  $\hat{g}_1(\hat{D}) = 0$  for  $\hat{D} < 0$ .

$$\hat{g}_0(\hat{D}) = \frac{\hat{D}^{(N+1/2)} N^{(N+3/2)} \mathcal{K}_{(3/2-N)}\left(\frac{\hat{D}N}{\sigma_w^2}\right)}{\sqrt{\pi} \Gamma(N) 2^{(N-3/2)} \sigma_w^{(2N+3)}} \quad (13)$$

In Figure 1,  $\hat{g}_0(\hat{D})$  is shown for different number of samples with noise power  $\sigma_w^2 = 1$ . As expected, increasing the number of samples in the sample covariance matrix reduces the variance of the PDF and also reduces the mean. Asymptotically, i.e. for  $N \rightarrow \infty$ , the test statistic  $D$  should be zero.

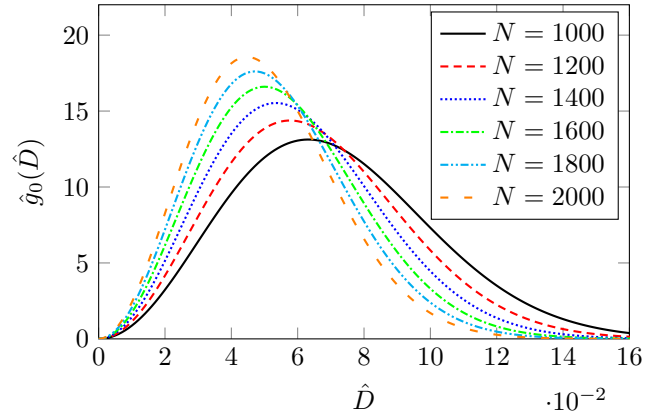


Fig. 1.  $\hat{g}_0(\hat{D})$  is plotted for different number of samples  $N$  and noise power  $\sigma_w^2 = 1$ .

The dependency of  $\hat{g}_0(\hat{D})$  on the noise power  $\sigma_w^2$  is depicted in Figure 2, where it can be seen that increasing  $\sigma_w^2$  affects the variance greatly and also shifts the mean away from zero.

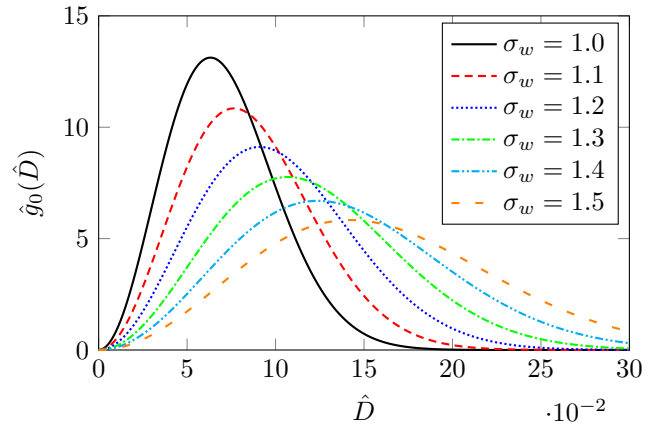


Fig. 2.  $\hat{g}_0(\hat{D})$  is plotted for different values of the noise power  $\sigma_w^2$  and  $N = 1000$  number of samples.

Figure 3 visualizes  $\hat{g}_0(\hat{D})$  together with  $\hat{g}_1(\hat{D})$  for different SNRs. Higher SNRs predominantly increase the mean of the PDF, while only slightly increasing the variance. Values obtained from a digital simulation of 50000 monte-carlo

$$g_1(D) = \frac{e^{-D} e^{-(2\alpha N)}}{2\alpha N \Gamma(N-1)} \sum_{j=0}^{\infty} \frac{(2\alpha N)^j D^{(j+2N-2)}}{\Gamma(j+1) \Gamma(j+N-1)} \times \left[ \int_0^{\infty} \Lambda^{(N-2)} (\Lambda+1)^{(j+N-2)} e^{-(2D\Lambda)} d\Lambda - \int_0^{\infty} \Lambda^{(j+N-2)} (\Lambda+1)^{(N-2)} e^{-(2D\Lambda)} d\Lambda \right] \quad (11)$$

$$g_1(D) = \frac{e^{-D} e^{-(2\alpha N)}}{\Gamma(N-1)} \sum_{j=0}^{\infty} \frac{(2\alpha N)^{(j-1)} D^{(j+2N-2)}}{\Gamma(j+1) \Gamma(j+N-1)} \times [\Gamma(N-1) \mathcal{U}(N-1, j+2N-2, 2D) - \Gamma(j+N-1) \mathcal{U}(j+N-1, j+2N-2, 2D)] \quad (12)$$

$$\hat{g}_1(\hat{D}) = \frac{e^{-\left(\frac{\hat{D}N}{\sigma_w^2}\right)} e^{-(2\alpha N)}}{\Gamma(N-1)} \sum_{j=0}^{\infty} \frac{(2\alpha N)^{(j-1)} N^{(j+2N-1)} \hat{D}^{(j+2N-2)}}{\Gamma(j+1) \Gamma(j+N-1) \sigma_w^{(2j+4N-2)}} \times \left[ \Gamma(N-1) \mathcal{U}\left(N-1, j+2N-2, \frac{2\hat{D}N}{\sigma_w^2}\right) - \Gamma(j+N-1) \mathcal{U}\left(j+N-1, j+2N-2, \frac{2\hat{D}N}{\sigma_w^2}\right) \right] \quad (14)$$

instances, where each covariance matrix was estimated from  $N = 1000$  samples, are drawn in circles for  $\hat{g}_0(\hat{D})$  and for  $\hat{g}_1(\hat{D})$  with  $\alpha = -13$  dB as an example. It is evident, that the empirical results confirm our theoretical findings.

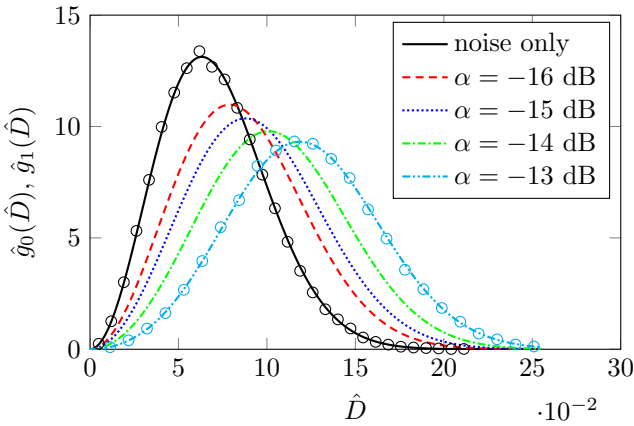


Fig. 3.  $\hat{g}_0(\hat{D})$  and  $\hat{g}_1(\hat{D})$  are plotted for different values of the SNR  $\alpha$ ,  $N = 1000$  number of samples and noise power  $\sigma_w^2 = 1$ . The circles indicate values obtained from a digital simulation.

#### IV. PERFORMANCE EVALUATION

Under the system model introduced in Section II, the PDFs for the MME detector as well as the PDFs for the MMME detector are now available for both hypotheses for  $K = 2$ . Although a CDF is known for the MME detector under Hypothesis  $\mathcal{H}_0$  [9], the other PDFs are either very complicated to integrate or an analytical form of the integral is unknown to us. However, having analytical expressions for the PDFs, numerical integration of the PDFs to obtain the CDFs works very well. Thus, we can compute the performance of both detectors in terms of the receiver-operator characteristic (ROC) by numerically calculating the CDFs, since it holds

for the probability of false-alarm  $P_{fa}^{MME}$  and the probability of detection  $P_d^{MME}$  of the MME detector:

$$P_{fa}^{MME}(h_{MME}) = 1 - F_0(h_{MME}) = 1 - \int_1^{h_{MME}} f_0(T) dT,$$

$$P_d^{MME}(h_{MME}) = 1 - F_1(h_{MME}) = 1 - \int_1^{h_{MME}} f_1(T) dT.$$

Here,  $h_{MME}$  is the threshold of the MME detector. Likewise,  $P_{fa}^{MMME}$  and  $P_d^{MMME}$  can be obtained for the threshold  $h_{MMME}$  for the MMME detector. In Figure 4, the ROCs for both the MME and the MMME detector are depicted for different SNRs,  $N = 1000$  number of samples and noise power  $\sigma_w^2 = 1$ . Again, we have drawn values resulting from a digital simulation of 50000 blocks in circles into the same figure. Firstly, the predicted performance is in total agreement to the empirical results. Secondly, the MMME detector shows a better performance than the MME detector, as was reported in [7].

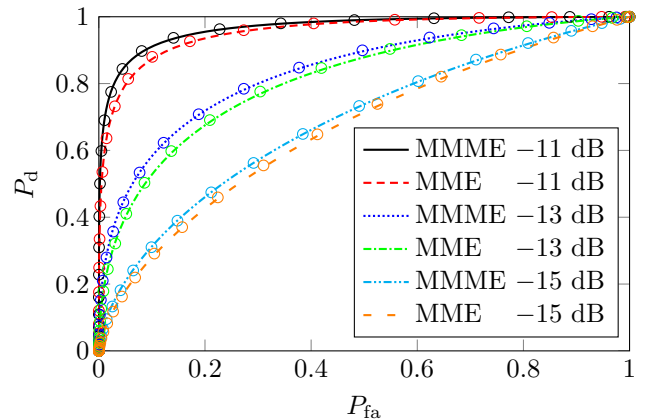


Fig. 4. ROC comparison between the MME and the MMME detector for different SNRs,  $N = 1000$  number of samples and noise power  $\sigma_w^2 = 1$ . The circles indicate values obtained from a digital simulation.

## V. NOISE UNCERTAINTY EVALUATION

We have shown that the MMME detector performs favorably compared to the MME detector in Section IV. However, as demonstrated in Section III-B, the test statistic of the MMME detector depends on the noise power  $\sigma_w^2$ . Since the precise noise power is usually unknown at the receiver, it must be estimated. For a robust detection the uncertainty of the noise power estimation must be taken into account when setting the detector threshold. Hence, the performance of the MMME detector will deteriorate as the noise power uncertainty increases. Naturally, the question arises how much noise uncertainty can be tolerated, so that the MMME detector still performs better or equal to the MME detector.

For this analysis, let  $\sigma_w^2$  and  $\alpha$  denote the actual noise power and SNR, respectively. The noise power estimation is assumed to return a value that is accurate within a bounded interval  $[(1/\rho)\sigma_w^2, \rho\sigma_w^2]$ . When designing the threshold  $h_{\text{MMME}}$ , it is usually desired to attain a false alarm rate that is below or equal to a predefined value. Thus, in order to have an upper bounded  $P_{\text{fa}}^{\text{MMME}}$ , the noise power must be assumed to be  $\rho\sigma_w^2$  to set the threshold robustly. For the following derivation we denote the CDFs of the MME detector and the MMME detector as  $F$  and  $G$ , respectively. Subscripts identify the corresponding Hypothesis  $\mathcal{H}_0$  or  $\mathcal{H}_1$ .

Suppose the threshold of the MME detector  $h_{\text{MME}}$  was set, so that the false-alarm rate is  $P_{\text{fa}}$ . In order to find the threshold of the MMME detector  $h_{\text{MMME}}$ , which results in the same detection performance, it must hold  $P_{\text{d}}^{\text{MME}} = P_{\text{d}}^{\text{MMME}}$  and hence  $h_{\text{MMME}} = G_1^{-1}(F_1(h_{\text{MME}}))$ . Then, we have to find  $\rho$ , such that  $G_0(h_{\text{MMME}}; \rho\sigma_w^2) \stackrel{!}{=} P_{\text{fa}}$ . Here,  $G_0(h_{\text{MMME}}; \rho\sigma_w^2)$  is the CDF of the MMME detector under Hypothesis  $\mathcal{H}_0$  evaluated for the upper bounded noise power instead of the true noise power. Deriving a closed-form expression for  $\rho$  is not possible, since closed-form expressions for the (inverse) CDFs are missing. However, similar to the ROC calculation,  $\rho$  can be found by numerical evaluation. For  $N = 1000$  number of samples, actual noise power  $\sigma_w^2$  the values found are summarized in Table I for different SNRs. If an estimation

TABLE I  
MAXIMUM NOISE UNCERTAINTY  $\rho$  TOLERABLE, SO THAT  
 $P_{\text{d}}^{\text{MMME}} \geq P_{\text{d}}^{\text{MME}}$  WITH UPPER BOUNDED  $P_{\text{fa}} \leq 0.01$

|        |           |           |           |
|--------|-----------|-----------|-----------|
| SNR    | −10 dB    | −11 dB    | −12 dB    |
| $\rho$ | 0.3904 dB | 0.3163 dB | 0.2563 dB |
| SNR    | −13 dB    | −14 dB    | −15 dB    |
| $\rho$ | 0.2062 dB | 0.1662 dB | 0.1321 dB |

of the noise power is available that is at least as accurate as summarized in Table I it would be beneficial to use the MMME detector instead of the MME detector. As an example, if the SNR is −11 dB, we can deduce from the table that the noise power estimate may be approx. 7.5% larger than the true value before the MMME detector starts to perform worse than the MME detector.

## VI. CONCLUSION

In this work, we have derived the test statistic PDFs of the MMME detector under both Hypotheses  $\mathcal{H}_0$  and  $\mathcal{H}_1$ . We use a simple AWGN model and assume one potentially present PU which transmits a PSK modulated signal. For  $K = 2$  cooperating secondary users, analytical expressions for the test statistic distributions of the MMME detector were derived. Analytical test statistic PDFs of the well-known MME detector under the same model for both Hypotheses are taken from the literature. Then, we compare their performance using a ROC, which is calculated numerically based on the available PDFs. It becomes evident that the MMME detector shows superior performance over the MME detector. However, the MMME detector is dependent on the noise power. Thus, we analyze how much noise power uncertainty can be tolerated, so that the MMME detector still performs favorably.

## REFERENCES

- [1] Q. Zhao and B. M. Sadler, "A survey of dynamic spectrum access," *IEEE Signal Processing Magazine*, vol. 24, no. 3, pp. 79–89, 2007.
- [2] E. Axell, G. Leus, E. Larsson, and H. Poor, "Spectrum Sensing for Cognitive Radio : State-of-the-Art and Recent Advances," *IEEE Signal Processing Magazine*, vol. 29, pp. 101–116, May 2012.
- [3] Y. Zeng and Y.-C. Liang, "Maximum-minimum eigenvalue detection for cognitive radio," in *IEEE 18th Annual International Symposium on Personal, Indoor and Mobile Radio Communication*, vol. 7, (Athens, Greece), pp. 1–5, 2007.
- [4] Y. Zeng and Y.-C. Liang, "Eigenvalue-based spectrum sensing algorithms for cognitive radio," *IEEE Transactions on Communications*, vol. 57, pp. 1784–1793, June 2009.
- [5] X. Yang, K. Lei, S. Peng, and X. Cao, "Blind detection for primary user based on the sample covariance matrix in cognitive radio," *IEEE Communications Letters*, vol. 15, no. 1, pp. 40–42, 2011.
- [6] J. Font-Segura, J. Riba, J. Villares, and G. Vazquez, "Quadratic sphericity test for blind detection over time-varying frequency-selective fading channels," in *2013 IEEE International Conference on Acoustics, Speech and Signal Processing (ICASSP)*, pp. 4708–4712, May 2013.
- [7] A. Bollig and R. Mathar, "MMME and DME: Two new eigenvalue-based detectors for spectrum sensing in cognitive radio," in *IEEE Global Conference on Signal and Information Processing (GlobalSIP)*, (Austin, USA), pp. 1210–1213, 2013.
- [8] A. Zanella, M. Chiani, and M. Z. Win, "On the marginal distribution of the eigenvalues of Wishart matrices," *IEEE Transactions on Communications*, vol. 57, no. 4, pp. 1050–1060, 2009.
- [9] M. Matthaiou, M. R. McKay, P. J. Smith, and J. A. Nossek, "On the condition number distribution of complex Wishart matrices," *IEEE Transactions on Communications*, vol. 58, no. 6, pp. 1705–1717, 2010.
- [10] W. Zhang, G. Abreu, M. Inamori, and Y. Sanada, "Spectrum sensing algorithms via finite random matrices," *IEEE Transactions on Communications*, vol. 60, no. 1, pp. 164–175, 2012.
- [11] M. Arts, A. Bollig, and R. Mathar, "Quickest Eigenvalue-Based Spectrum Sensing using Random Matrix Theory," *ArXiv e-prints arXiv:1504.01628 [cs.IT]*, Apr. 2015.
- [12] A. T. James, "Distributions of matrix variates and latent roots derived from normal samples," *The Annals of Mathematical Statistics*, vol. 35, no. 2, pp. 475–501, 1964.
- [13] A. Kortun, T. Ratnarajah, M. Sellathurai, C. Zhong, and C. Papadias, "On the Performance of Eigenvalue-Based Cooperative Spectrum Sensing for Cognitive Radio," *IEEE Journal of Selected Topics in Signal Processing*, vol. 5, pp. 49–55, Feb. 2011.
- [14] A. Jeffrey and D. Zwillinger, *Table of integrals, series, and products*. Academic Press, 2007.
- [15] M. Matthaiou, D. I. Laurenson, and C.-X. Wang, "On analytical derivations of the condition number distributions of dual non-central Wishart matrices," *IEEE Transactions on Wireless Communications*, vol. 8, no. 3, pp. 1212–1217, 2009.
- [16] M. Abramowitz, I. A. Stegun, and others, *Handbook of mathematical functions*, vol. 1. Dover New York, 1972.